Research Square

Preprints are preliminary reports that have not undergone peer review.
They should not be considered conclusive, used to inform clinical practice,
or referenced by the media as validated information.

Structural, spectroscopic and DFT insights into intermolecular interactions of caffeine-malonic acid cocrystal

Priya Verma

priyaverma220192@gmail.com

University of Lucknow

Anubha Srivastava

University of Lucknow

Preeti Prajapati

University of Lucknow

Poonam Tandon

University of Lucknow

Uma Sharma

Vikram University

Manishkumar R. Shimpi

Luleå University of Technology

Research Article

Keywords: Caffeine, malonic acid, caffeine-malonic acid cocrystal, hydrogen bonding, chemical reactivity.

Posted Date: November 23rd, 2026

DOI: https://doi.org/10.21203/rs.3.rs-11566464/v1

License: This work is licensed under a Creative Commons Attribution 4.0 International License.
Read Full License

Additional Declarations: No competing interests reported.

Structural, spectroscopic and DFT insights into intermolecular interactions of caffeine-malonic acid cocrystal

Priya Verma[1], Anubha Srivastava[1*], Preeti Prajapati[1], Meenu Purohit[3], Poonam Tandon[1,2*], Uma Sharma[3], Manishkumar R. Shimpi[4]

[1*]*Department of Physics, University of Lucknow, Lucknow, 226007, India.*
[2*]*Department of Physics, Deen Dayal Upadhyaya Gorakhpur University, Gorakhpur, 273009, India.*
[3] *School of studies in Chemistry and Biochemistry, Samrat Vikramaditya University, Ujjain, 456010, India.*
[4]*Chemistry of Interfaces, Luleå University of Technology, SE-971 87, Luleå, Sweden.*

***Correspondence:**

Poonam Tandon: tandon_poonam@lkouniv.ac.in
Priya Verma: priyaverma220192@gmail.com

Abstract

The present study aims to investigate the hydrogen bonding interactions, vibrational characteristics, physicochemical properties and structure-activity relationship of caffeine-malonic acid (CAF-MA) cocrystal by using both computational and experimental approaches. The CAF-MA cocrystal was prepared by the solvent-assisted grinding method. PXRD analysis confirmed the generation of CAF-MA cocrystal. The theoretical study of the CAF-MA cocrystal was carried out using two models, namely the CAF-MA cocrystal monomer (2:1) and (monomer+1MA) (2:2), with the aid of the DFT/CAM-B3LYP/6-311++G(d,p) method. The (monomer+1MA) model was designed to cover the nearest possible hydrogen bonding interactions observed in the crystal structure of CAF-MA cocrystal. The experimental and theoretical spectral analyses of cocrystal show that strong intermolecular hydrogen bonds; (O25-H26⋯N7), (O66-H67⋯O39) and (O31-H32⋯O39) are present in the (monomer+1MA) of CAF-MA cocrystal. Bader's quantum theory of atoms in molecules (AIM) was employed to analyze the strength and nature of all the intra- and intermolecular hydrogen bonds. The HOMO-LUMO energy gap of (monomer+1MA) of CAF-MA cocrystal (7.4233 eV) < CAF (7.7420 eV), hence CAF-MA cocrystal has higher chemical reactivity than CAF. Overall, the present study provides a reliable understanding of the structural and electronic features of the CAF-MA cocrystal and may serve as a useful basis for the exploration and design of new pharmaceutical cocrystal systems in the future.

Keywords

Caffeine; malonic acid; caffeine-malonic acid cocrystal; hydrogen bonding; chemical reactivity.

1. Introduction

Pharmaceutical cocrystals have emerged as an effective crystal engineering strategy for improving the physicochemical properties of active pharmaceutical ingredients (APIs) without altering their pharmacological activity [1, 2]. Consequently, they have gained considerable attention as an attractive approach for the development and optimization of pharmaceutical solid forms [3, 4]. Sakhiya et al. [5] reviewed recent advances in pharmaceutical cocrystallization and highlighted the importance of modern characterization techniques for understanding cocrystal formation. Pantwalawalkar et al. [6] emphasized the growing role of pharmaceutical cocrystals in improving the physicochemical performance of challenging drug candidates.

Recent advances in vibrational spectroscopy have significantly improved the molecular-level characterization of pharmaceutical cocrystals. In particular, Raman spectroscopy has emerged as a powerful complementary technique to FT-IR for identifying polymorphic transformations, monitoring cocrystal formation in real time, and investigating intermolecular interactions responsible for crystal stability [7, 8]. In addition, terahertz time-domain spectroscopy (THz-TDS) has attracted considerable attention because it directly probes low-frequency intermolecular vibrations associated with crystal packing and hydrogen-bonding networks, thereby providing unique insights into cocrystal formation and polymorphism that are not readily accessible by conventional vibrational techniques [9, 10]. The combined use of PXRD, FT-IR, Raman spectroscopy, terahertz spectroscopy, and Density functional theory (DFT) calculations has therefore become a modern strategy for establishing reliable structure-property relationships in pharmaceutical cocrystals [11-15].

Although several caffeine-based cocrystals with organic acids and other pharmaceutical coformers have been reported, most previous studies have primarily focused on crystal synthesis, crystal structure determination, and improvements in physicochemical properties [16, 17]. Trask et al. prepared, experimentally synthesized and predicted hydrogen bonding patterns in various cocrystals of CAF with oxalic acid, glutaric acid, malonic acid and maleic acid [18]. The cocrystals of theophylline and glibenclamide have been reported with malonic acid as coformer to study solubility and hygroscopic behavior [19, 20]. Several cocrystals of caffeine (API) with sulfacetamide [21], sedative barbital [22] and citric acid [23] (coformers) have been studied in literature.

A comprehensive molecular-level investigation correlating vibrational spectroscopic signatures with hydrogen-bonding synthons, charge-transfer interactions, electronic structure, and chemical reactivity of the caffeine-malonic acid (CAF-MA) cocrystal is still lacking. Furthermore, theoretical studies integrating AIM, NBO, frontier molecular orbital and molecular electrostatic potential analyses with experimental spectroscopic characterization have not been reported for this cocrystal. Therefore, a detailed understanding of the structure-interaction-property relationship governing the CAF-MA cocrystal remains an important research challenge. CAF-MA cocrystal exists in orthorhombic structure with the space group Fdd2 and with unit cell parameters a= 30.3992, b= 31.2845, c= 4.6739, α= 90˚, β= 90˚, γ= 90˚ [18]. The chemical structures of cocrystallizing agents (CAF and MA) are presented in Fig. 1(a) and 1(b), respectively.

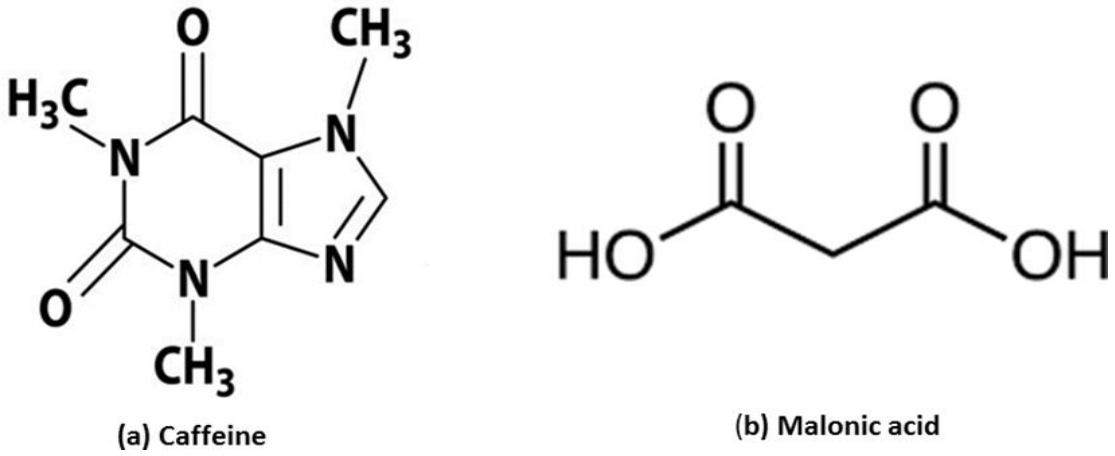

Fig. 1. The chemical structures of cocrystallizing entities; (a) caffeine, (b) malonic acid.

The present study aims to establish a comprehensive structure-interaction-property relationship for the caffeine-malonic acid (CAF-MA) cocrystal through an integrated experimental and theoretical investigation. The cocrystal was synthesized by the solvent-assisted grinding method and characterized using PXRD, FT-IR, and FT-Raman spectroscopy. The crystal structures of CAF, MA and CAF-MA cocrystal were given in Figs. S1-S3, respectively. To obtain molecular-level insight into cocrystal formation, two computational models, namely the monomer (2:1) and (monomer+1MA) (2:2), were investigated using the DFT/CAM-B3LYP/6-311++G(d,p) method. Detailed vibrational spectroscopic investigation has been successfully made to study the groups actively involved in the formation of cocrystal by noticing the significant changes in their wavenumbers and bond lengths. AIM and NBO analyses were employed to elucidate the nature and strength of intra- and intermolecular hydrogen bonds, while frontier molecular orbital analysis, global reactivity descriptors, and molecular electrostatic potential mapping evaluation were performed to understand the electronic structure and physicochemical behavior of the cocrystal. By correlating the experimental vibrational spectra with quantum chemical analyses, this work provides a comprehensive molecular-level understanding of the CAF-MA cocrystal

and offers valuable insights for the rational design of pharmaceutical cocrystals with improved functional properties.

2. Experimental details

Anhydrous CAF, MA and methanol (purity, 99%) were purchased from Sigma-Aldrich GmbH. Solid-state grinding experiments were carried out manually using a Retsch MM500 Mixer Mill, equipped with 10 mL stainless steel grinding jars and two 7 mm stainless steel balls per jar. The grinding process was performed at a frequency of 30 Hz for 30 minute. To obtain the CAF-MA cocrystal, solvent-assisted grinding was conducted under the same conditions (30 Hz, 30 minutes) using 10 μL of methanol. The mixture contained CAF (0.388 g, 2 mmol) and MA (0.104 g, 1 mmol). After 30 minutes, the solids were isolated and subjected to PXRD.

2.1 Powder X-ray diffraction (PXRD) analysis

PXRD patterns for the samples were collected on an Empyrean X-ray diffractometer (PANalytical, The Netherlands) equipped with a monochromatic Cu Kα1 radiation X-Ray tube (λ=1.54056 Å) and PIXel3D detector. The amperage and tube voltage were put at 40 mA and 45 kV, respectively. Samples were prepared by filling onto a metal sample holder and compressed. Silicon reference standard was used for Instrument calibration. The sample was scanned by using 2θ range of 5–40º, increasing by a step size of 0.026 at 25 ºC. The data were processed by HighScore Plus software (PANalytical, The Netherlands). Same experimental setup has been used in the earlier publication [24].

2.2 Infrared spectral analysis

Infrared spectra were recorded on a Bruker Vertex 80v FTIR spectrometer fitted with a DLaTGS detector and a diamond crystal as ATR element with a Platinum-ATR accessory. Both the single beam spectra of the powered samples and a single beam background without sample were obtained by an optical resolution of 4 cm^{-1} with averaging 128 scans. Same as performed in the previously published articles [24, 25].

2.3 Raman spectral analysis

As reported by Shimpi et al. [25], the Raman spectra were recorded using a Chromex Sentinel dispersive Raman unit equipped with a TE cooled CCD and 785 nm, 70 mW excitation laser. Each spectrum is resulted in twenty co-added 20 second scans. The unit has continuous automatic calibration with an internal standard. The data was collected through SentinelSoft data acquisition software and further processed in GRAMS AI.

3. Computational and theoretical details

All computational calculations were completed by employing density functional theory (DFT) and long-range-corrected hybrid functional (CAM-B3LYP) [13, 14] along with 6-311++G(d,p) basis set [26, 27]. The primary aim of the geometry optimization is to obtain minimum energy of the molecule, so as to find the stable structure and electronic behavior of CAF, MA, monomer and (monomer+1MA) models of CAF-MA cocrystal set by Gaussian 09 program [28]. The optimized structures were visualized by use of GaussView tool [29].

Pulay et al., defined a complete set of all the internal coordinates. The assignments were done on the basis of potential energy distribution (PED) analysis [30, 31], calculated by using Gar2Ped software package [32].

Topological and geometrical parameters for bonds of interacting atoms and their molecular graphs have been obtained by using AIMALL software [33] and pictured by AIM2000 [34]. Espinosa defined the proportionality between hydrogen bond energy (E_{HB}) and potential energy density (V_{BCP}) at H···O contact by the expression, $E_{HB} = 0.5\ V_{BCP}$ [35].

The NBO calculations were performed using the same level of methodology. The stabilization energy, $E^{(2)}$ was estimated for NBO calculations from second-order perturbation approach [36].

The ionization potential (I) and electron affinity (A), electronegativity (χ), chemical hardness (η), chemical potential (μ), global softness (S) and electrophilicity index (ω) [37-40] values may be defined as:

$$I = -E_{HOMO} \quad (1)$$

$$A = -E_{LUMO} \quad (2)$$

$$\chi = \frac{(I+A)}{2} \quad (3)$$

$$\eta = \frac{(I-A)}{2} \quad (4)$$

$$\mu = -\frac{(I+A)}{2} \quad (5)$$

$$S = \frac{1}{2\eta} \quad (6)$$

$$\omega = \frac{\mu^2}{2\eta} \quad (7)$$

The maximum electronic charge (ΔN_{max}) that is accepted by an electrophile may be represented as;

$$N_{max} = -\frac{\mu}{\eta} \quad (8)$$

The charge transfer between two interacting i.e. electrophilic charge transfer (ECT) of two molecules P and Q may be calculated as:

$$ECT = (\Delta N_{max})_P - (\Delta N_{max})_Q \qquad (9)$$

Where, $(\Delta \boldsymbol{N_{max}})_{\boldsymbol{P}} = -\frac{\boldsymbol{\mu_P}}{\boldsymbol{\eta_P}}$ **and** $(\Delta \boldsymbol{N_{max}})_{\boldsymbol{Q}} = -\frac{\boldsymbol{\mu_Q}}{\boldsymbol{\eta_Q}}$

4. Results and discussion

4.1 Geometry optimization and energies

The optimized ground state structures and their geometries were obtained by the application of DFT method with the aid of Coulomb-attenuated hybrid exchange-correlation functional (CAM-B3LYP) [13, 14] and 6-311++G(d,p) [26] basis set by using Gaussian 09 program package [28]. The initial geometries of CAF, MA, monomer and (monomer+1MA) of CAF-MA cocrystal were taken from their reported crystal structures, to the perform computations. The ground state optimized structures of CAF, MA, monomer and (monomer+1MA) were shown in Figs. S4, S5 (ESI), 2 and 3, respectively. The optimized parameters of CAF, MA, monomer and (monomer+1MA) with their respective experimental values were tabulated in Table S1. The optimized structures were also presented in XYZ format in Tables S2 and S3 (ESI), respectively.

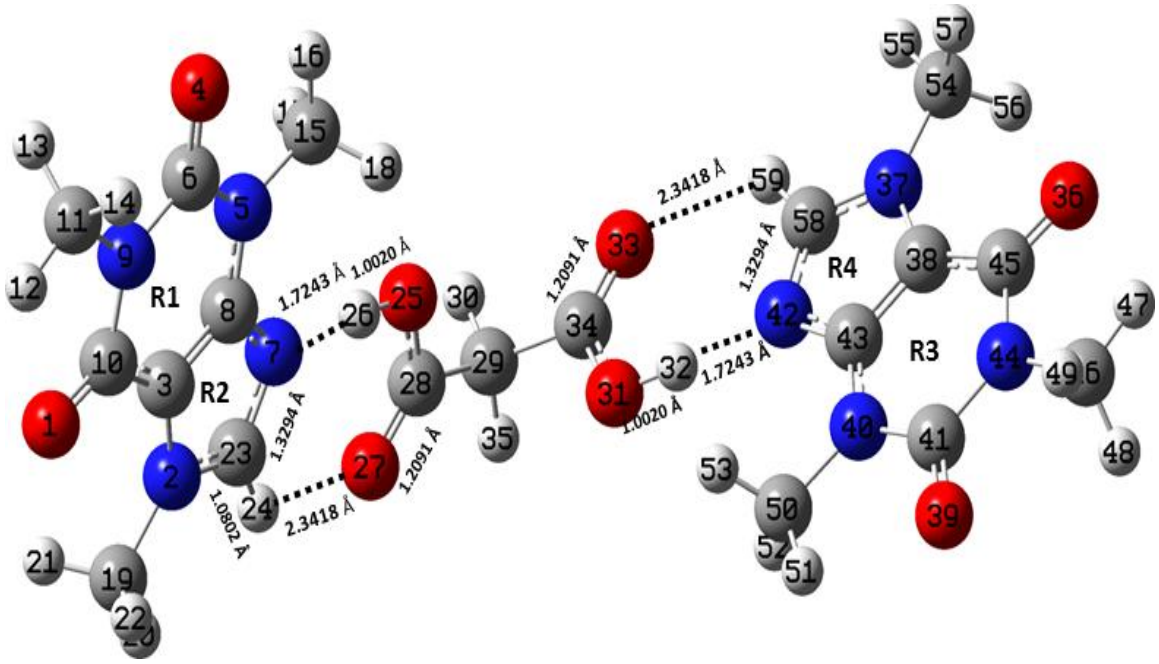

Fig. 2. Optimized structure for monomer model of CAF-MA cocrystal with the atomic numbering scheme adopted in the present study.

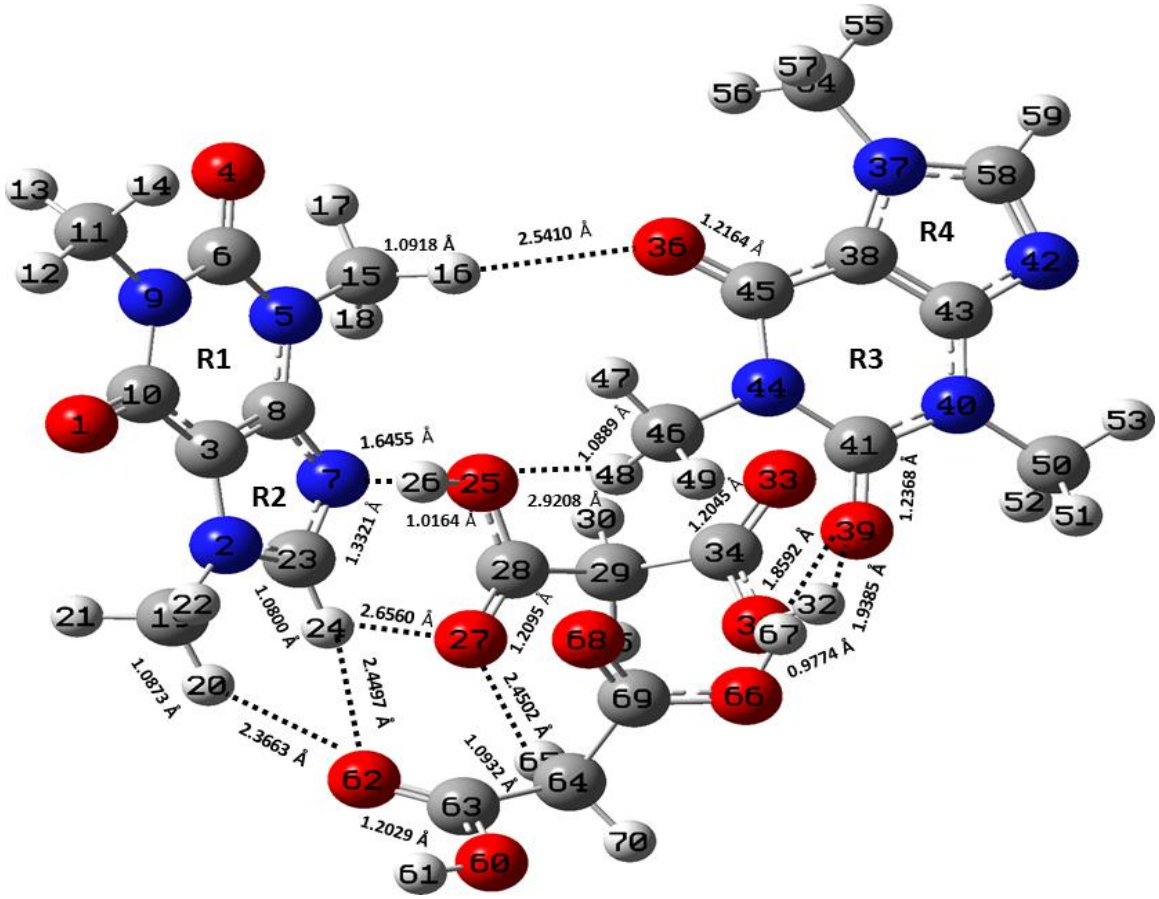

Fig. 3. Optimized structure for (monomer+1MA) model of CAF-MA cocrystal with the atomic numbering scheme adopted in the present study.

The optimized geometrical parameters of CAF and monomer of CAF-MA cocrystal were compared with each other. It was pointed out that the calculations do not replicate the values 0.1364 Å in bond-lengths of (O36=C45) bond, 14.79/14.73° in bond-angles for (C3-C10-N9)/(O36=C45-C38) bonds and 0.59° in dihedral-angles for (C10-N9-C11-H14), without the bonds having hydrogen atom. Additionally, the larger differences in bonds; (N2-C23), (N7-C23), (N37-C58) and (N42-C58) were 0.0069, 0.007, 0.0069 and 0.007 Å, respectively. This was due to presence of intermolecular hydrogen bonds (N7···H26-O25), (C23-H24···O27), (C58-

H59⋯O33) and (N42⋯H32-O31), respectively with neighboring molecules in monomer model of cocrystal (shown in Fig. 2 and Table S1).

Similarily, the computed parameters of MA were compared with the monomer of CAF-MA cocrystal, differences of 0.0052 Å in (C28-C29), 1.77° in (C28-C29-C34) and 11.8° in (O25-C28-C29-H35) have been initiated in the respective bond-lengths, bond-angles and dihedral angles, respectively, except for the bonds with hydrogen atom. However, the major differences in bonds of (O25-H26), (O27=C28), (O31-H32) and (O33=C34), were 0.0342, 0.0114, 0.0341 and 0.0122 Å, respectively due to the involvement of these bonds in intermolecular hydrogen bonding (N7⋯H26-O25), (C28=O27⋯H24), (N42⋯H32-O31) and (C58-H59⋯O33), respectively (as shown in Fig. 2).

The simulated parameters of monomer/ (monomer+1MA) of CAF-MA cocrystal were compared with their respective experimental values [18]. The geometrical parameters show that the calculations do not differ more than by 0.0789/0.0763 Å in bond-lengths of (C29-H30), 4.41/1.28° in bond-angles of (C28-C29-C34) and 4.41/1.69° in dihedral angles of (C15-N5-C6=O4), except for those involved in hydrogen bonding and one of the atom as a hydrogen.

A comparison of calculated geometrical parameters of monomer and (monomer+1MA) show that the (monomer+1MA) (as pictured in Fig. 3) matched well with the experimental parameters due to considerations of nearest possible interactions, as in crystal structure of cocrystal (having bulk state interactions) (as shown in Fig. S3).

4.2 Powder X-ray diffraction (PXRD)

The formation of the CAF-MA cocrystal was confirmed by PXRD. The experimental PXRD pattern of the product obtained by solvent-assisted grinding shows excellent agreement with the

simulated PXRD pattern generated from the reported crystallographic information file for the 2:1 caffeine-malonic acid cocrystal crystallizing in the orthorhombic space group [18]. As illustrated in Fig. 4, all characteristic reflections of the simulated pattern are reproduced in the experimental data, with no additional peaks observed. This close correspondence confirms successful cocrystal formation and demonstrates that the obtained material is a single-phase, X-ray-pure cocrystal [18].

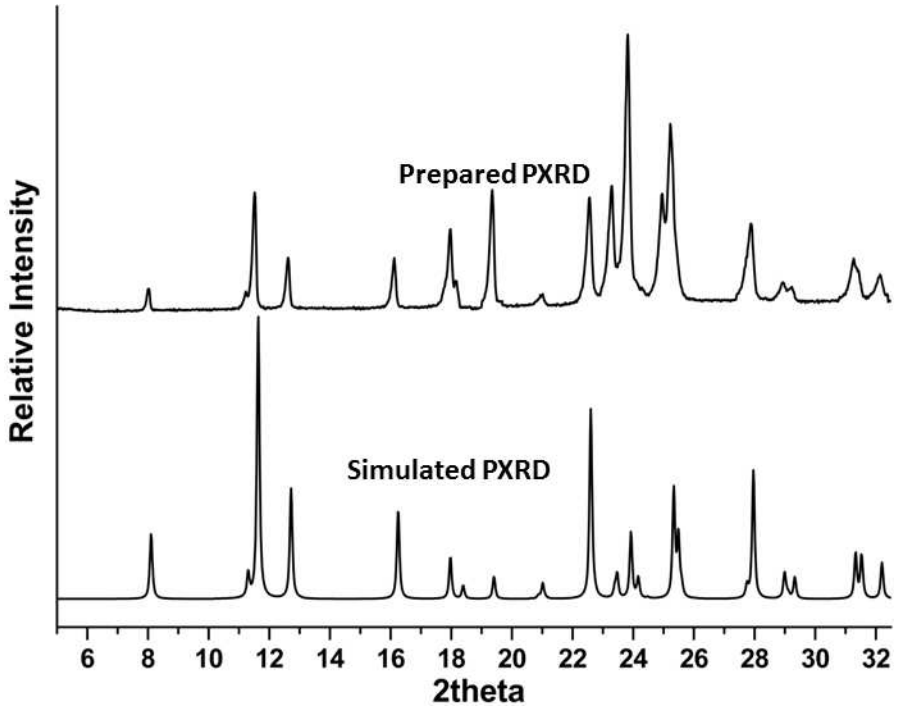

Fig. 4. PXRD pattern of prepared CAF-MA cocrystal (**top**) and the simulated PXRD pattern generated from known crystal structure form (**bottom**).

4.3 Spectroscopic analysis and wavenumbers

Vibrational spectroscopic analyses with theoretical calculations are used to describe the chemical bonds in molecular system [41, 42]. CAF and MA exhibits monoclinic and triclinic space group, crystallize into Cc and P-1 space group, respectively [43, 44]. The total number of atoms in

CAF, MA, monomer and (monomer +1MA) is 24, 11, 59 and 70, which suggest that these can produce 66, 27, 171 and 204 (3N-6) normal modes, Raman and IR active modes, respectively. The theoretical and experimental vibrational of CAF, MA and monomer/(monomer+1MA) of CAF-MA cocrystal achieved by CAM-B3LYP/6-311++G(d,p) with their potential (PED) analysis were tabulated in Tables S4, S5 and S6, respectively. The combined experimental and theoretical IR/Raman spectra of CAF and MA were shown in Figs. S6/S7 and S8/S9, respectively. Additionally, the comparison between IR and Raman spectra for monomer and (monomer+1MA) of cocrystal with experimental spectra were shown in Table 1 and Figs. 5 and 6, respectively.

Table1 Observed and calculated bond-length (Å) and stretching frequency (cm^{-1}) of modes of CAF, MA, monomer and (monomer+1MA) of CAF-MA cocrystal involved in hydrogen bonding.

	Groups present in CAF				Groups present in MA			
	C-N of imidazole ring		C-H group of imidazole ring		C=O group		O-H group	
Molecules	**Bond-length**	**Stretching frequency**	**Bond-length**	**Stretching frequency**	**Bond-length**	**Stretching frequency**	**Bond-length**	**Stretching frequency**
				Experimental				
CAF	1.3282	1325,1325 (IR, Raman)	1.0000	3111,3114 (IR, Raman)	-	-		
MA	-	-	-	-	1.2205	1691, 1684 (IR, Raman)	0.8201	3627 (Raman)
					1.2256	1691, 1684 (IR, Raman)	0.8197	3608 (Raman)
CAF-MA cocrystal	1.3408	1336,1339 (IR, Raman)	0.9497	3118,3119 (IR, Raman)	1.2024	1713,1721 (IR, Raman)	1.0363	2977,2972 (IR, Raman)
			0.9497	3114 (Raman)	1.2024	1710, 1716 (IR, Raman)	1.0363	2948,2950 (IR, Raman)
				Theoretical				
CAF	1.3224	1330 (C14-N6)	1.0797	3108 (C14-H15)	-	-		
MA	-	-	-	-	1.1977	1788 (C11=O4)	0.9678	3622 (O5-H6)
					1.1969	1771 (C7=O1)	0.9679	3619 (O2-H3)
monomer model of cocrystal	1.3294	1346 (C23-N7)	1.0802	3112 (C23-H24)	1.2091	1734 (C34=O33)	1.0020	2972 (O31-H32)
	1.3294	1346	1.0802	3112 (C58-H59)	1.2091	1717	1.0020	2949 (O25-H26)

		(C58-N42)				(C28=O27)		
(monomer+1MA) of cocrystal	1.3321	1343 (C23-N7)	1.0800	3117 (C23-H24),	1.2045	1734 (C34=O33)	0.9800	2974 (O31-H32)
	1.3223	1339 (C58-N42)	1.0797	3110 (C58-H59)	1.2095	1713 (C28=O27)	1.0164	2944 (O25-H26)

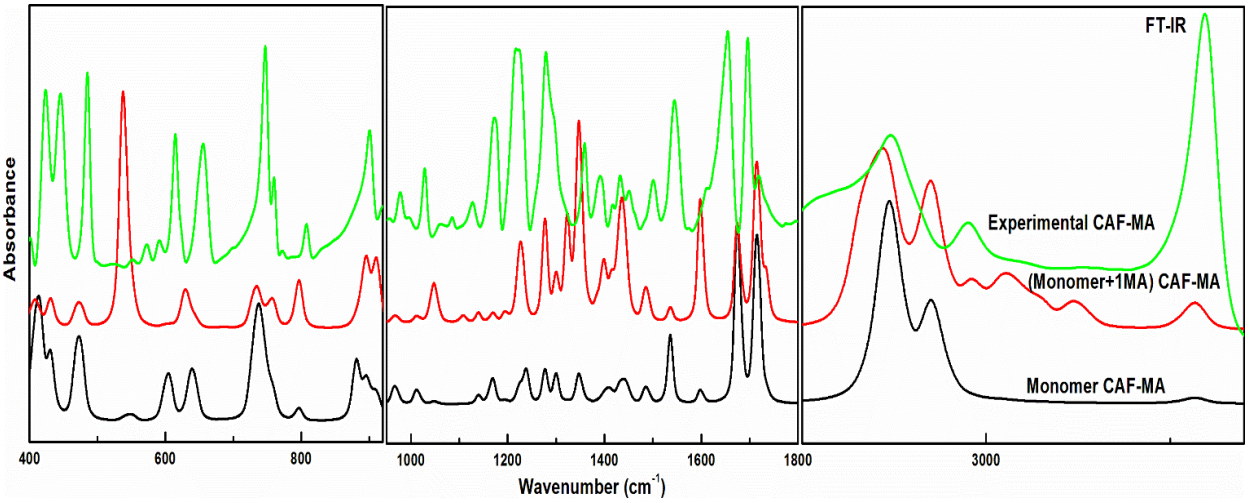

Fig. 5. Experimental and calculated (scaled) IR absorbance spectra of monomer and (monomer+1MA) of cocrystal in the region 400-920 cm^{-1}, 900-1800 cm^{-1} and 2900-3140 cm^{-1}.

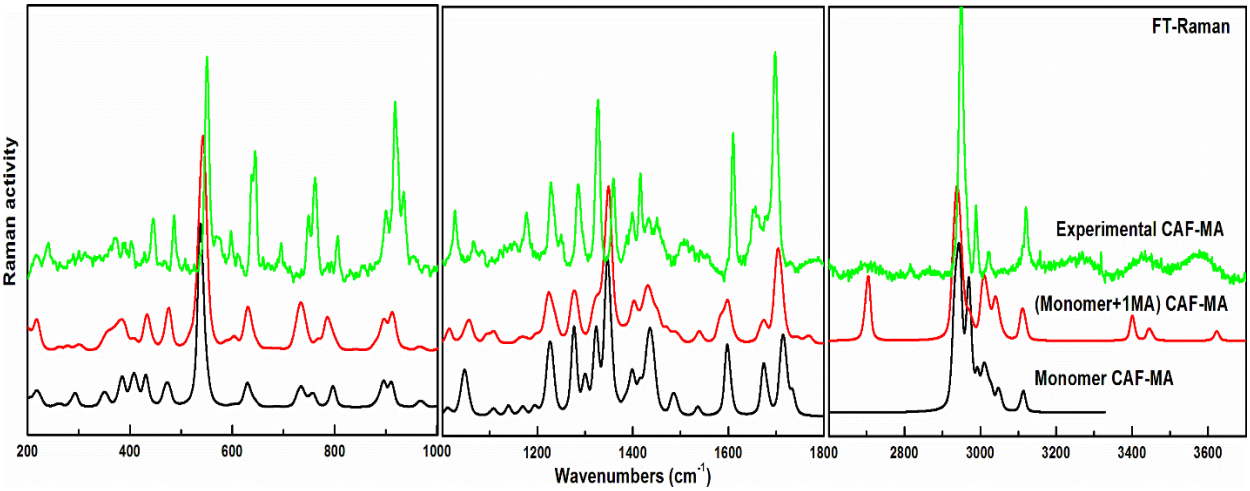

Fig. 6. Experimental and calculated (scaled) Raman scattering spectra of monomer and (monomer+1MA) model of cocrystal in the region 200-1001 cm^{-1}, 1001-1800 cm^{-1} and 2601-3700 cm^{-1}.

The differences between the simulated and the experimental wavenumbers were due to the ignorance of anharmonic effects and isolated molecule calculations. So, the calculated wavenumbers were higher than experimental values. To overcome this error in CAM-B3LYP/6-311++G(d,p) method, the stretching wavenumbers were scaled down by factor 0.953 ubiquitously [45]. It was found that (C23-N7) and (C58-N42) of CAF with (O25-H26) and (O31-H32) of MA, respectively were forming strong hydrogen bonds (O25-H26⋯N7) and (O31-H32⋯N42). Furthermore, the weak intermolecular hydrogen bonds; (C23-H24⋯O27) and (C58-N42⋯H32) were formed in between CAF and MA in the crystal structure of CAF-MA cocrystal.

4.3.1 Ring vibrations of CAF

CAF molecule consists of one six membered pyrimidine and five membered imidazole rings. The (C-H) ring vibration modes of imidazole ring are assigned in the region of 3000-3100 cm^{-1} in IR and Raman spectra [46]. The C-H stretching modes of imidazole ring (R2) of individual CAF was calculated at 3108 cm^{-1} and observed with the IR/Raman peaks at 3111/3114 cm^{-1}.

In the monomer/(monomer+1MA) of CAF-MA cocrystal, the vibrational band were simulated at 3112/3117 cm^{-1} , respectively corresponding to observed peaks at 3118/3119 cm^{-1} in IR/Raman spectra. The vibrational modes of in-plane CH bending deformation are typically lie in the 900-1200 cm^{-1} region [47, 48]. Furthermore, a C-H out-of-plane bending vibration peaks at 750 cm^{-1} approximately [47]. These in-plane modes of CAF, monomer/(monomer+1MA) were attributed at 1170, 1169/1174 cm^{-1} with IR/Raman peaks at 1186/1186, 1172/1170 cm^{-1}, respectively. The C-H out-of-plane bending vibrations were calculated and observed at 834 and 830/830 cm^{-1}, respectively for individual CAF (tabulated in Table S4). While in monomer and

(monomer+1MA) of CAF-MA cocrystal, the same out-of-plane bending vibrations were calculated at 882 and 881 cm^{-1}, with corresponding assigned peak at 882 cm^{-1} in Raman spectra (given in Table S6).

It was noted that in pyrimidine ring R1 of CAF, the trigonal deformation was recorded at IR/Raman peaks at 631/631 cm^{-1} with corresponding calculated value at 627 cm^{-1}. The R1 asymmetric deformation was simulated at 469 cm^{-1} and observed at 455/455 cm^{-1} at IR/ Raman spectra. The puckering mode of ring was calculated at 149 cm^{-1} and observed at 144 cm^{-1} in Raman spectrum. The asymmetric torsion of this ring was simulated/ observed at 109/106 cm^{-1} in Raman spectrum region in individual CAF (given in Table S4).

4.3.2 Discussions of functional groups involved in hydrogen bonding

The noticeable changes in stretching wavenumbers and bond-lengths were observed in the functional groups which were directing the cocrystal formation between two constituents CAF and MA. From Fig. 2, it was clear that C-N and (C-H) of imidazole rings R2 and R4 of CAF were forming intermolecular hydrogen bonds with (O-H) and (C=O) of MA, respectively.

4.3.2.1 Hydroxyl (O-H) group of MA

The MA molecule consists of hydroxyl groups and these are found to be hydrogen bonded with neighbouring CN group of rings R2 and R4 of CAF in CAF-MA cocrystal [18]. In MA, two broad (O5-H6)/(O2-H3) peaks were observed at 3627/3608 cm^{-1} in IR spectrum, which were calculated at 3622/3619 cm^{-1}, respectively (as given in Table S5). In monomer, the (O31-H32)/(O25-H26) groups stretching vibrations were simulated at 2972/2949 cm^{-1}, which were assigned to IR/Raman peaks at 2977/2972 and 2948/2950 cm^{-1}, respectively. Additionally, in

(monomer+1MA) cocrystal, the same stretching vibrations of (O31-H32)/(O25-H26) groups were calculated at 2974/2944 cm^{-1}, respectively corresponding to same observed values.

It is noteworthy that the (O-H) groups were free from bonding in individual MA, but these groups were involved in intermolecular hydrogen bonds in monomer and (monomer+1MA) due to downward (red) shifting in calculated wavenumbers of 650/670 cm^{-1} and 648/675 cm^{-1} with increment in bond-lengths of 0.0341/0.0342 Å and 0.0485/0.0696 Å, respectively from MA, confirming the presence of intermolecular hydrogen bonding (C23-N7⋯H26-O25) and (C43-N42⋯H32-O31) in between CAF and MA.

4.3.2.2 Carbonyl (C=O) group of MA

The (C=O) group stretching vibrations present in the region of 1700-1800 cm^{-1} [48]. In MA, the (C11=O4)/(C7=O1) groups were simulated and assigned at 1788/1771 cm^{-1} and 1691/1684 cm^{-1} in IR/Raman peaks values (as depicted in Figs. S8 and S9).

In monomer and (monomer+1MA), the carbonyl groups (C34=O33)/(C28=O27) were involved in intermolecular hydrogen bonds, since the stretching vibrations of these groups were calculated at 1734/1717 cm^{-1} and 1734/1713 cm^{-1}, which corresponds to observed IR/Raman peaks at 1713/1721 and 1710/1716 cm^{-1}, respectively (given in Table S6). In monomer the lowering in calculated stretching vibrations of 54/54 cm^{-1} along with bond-lengths elongation of 0.0114/0.0165 Å, respectively from individual MA, revealing the presence of intermolecular hydrogen bonds (C23-H24⋯O27=C28) and (C58-H59⋯O33=C34), as shown in Fig. 2.

Similar kinds of changes were seen in the stretching wavenumbers of (monomer+1MA) of cocrystal. The stretching vibrations of (C34=O33)/(C28=O27) groups were generated the red shifting between calculated wavenumber values of 54/58 cm^{-1}, and with increment in calculated

bond-length values of 0.0160/0.0161 Å, from MA respectively, confirming these groups in the cocrystal formation.

4.3.2.3 C-N of imidazole ring of CAF

The recognition of stretching vibrations of (C-N) are strenuous task, because they are mixed with several other bands [49]. In CAF, the stretching vibration of (C14-N6) was calculated at 1330 cm^{-1} with corresponding observed peaks at 1325/1325 cm^{-1} in IR/Raman peaks. The same (C23-N7) stretching vibrations in monomer and (monomer+1MA) of CAF-MA cocrystal were simulated at 1346 and 1339 cm^{-1} corresponding to the IR/Raman spectra at 1336/1339 cm^{-1}, respectively. Since the (C-N) of imidazole ring is involved in intermolecular hydrogen bonds (N7⋯H26-O25) and (N4⋯H32-O31) with MA (as shown in Fig. 2). The strength of intermolecular hydrogen bond (N7⋯H26-O25) in (monomer+1MA) is stronger than monomer of CAF-MA cocrystal, as the bond distance in (monomer+1MA) (1.6455 Å) > (monomer) (1.7243 Å).

4.3.2.4 Methyl (CH_3) vibrations of CAF

CAF molecule consists of three $C13H_3$ groups; two of them attached with pyrimidine ring (R1) and one with imidazole ring (R2) (as depicted in Fig. S4). The asymmetric vibrations of the $C13H_3$ was observed at 3028/3023 cm^{-1} in IR/Raman spectra, which corresponds to calculated peak 3021 cm^{-1}. In monomer/(monomer+1MA) of CAF-MA cocrystal, the same stretching vibrations of same group ($C19H_3$) were calculated at 3028/3040 cm^{-1} corresponding to the observed stretching peak at 3039/3038 cm^{-1} in IR/Raman spectra, respectively.

Another asymmetric stretching vibration ($C11H_3$) of CAF was calculated at 3049 cm^{-1} with IR/Raman spectra at 3054/3054 cm^{-1}, respectively. In monomer/(monomer+1MA), these

stretching vibrations were calculated at 3051/3060 cm^{-1} with observed peaks at 3051/3052 cm^{-1} in IR/Raman spectra.

The symmetric stretching vibrations of $C13H_3$ of CAF were calculated at 2941 cm^{-1} with IR/Raman spectra at 2954/2958 cm^{-1}. Whereas in monomer/(monomer+1MA) were calculated at 2943/2943 cm^{-1} with corresponding IR/Raman peaks at 2944/2947 cm^{-1} in IR/Raman spectra, respectively (as given in Table S6). The symmetric stretching vibrations of $C13H_3$ group of CAF were calculated at 2939 cm^{-1} with observed IR/Raman spectra at 2903/2903 cm^{-1}. In monomer/(monomer+1MA), the stretching vibrations of ($C19H_3$) group were calculated at 2942/2940 cm^{-1} with corresponding IR/Raman peaks at 2944/2947 cm^{-1}, respectively.

4.3.2.5 Methylene (CH_2) group of MA

The stretching vibrations of CH_2 group are usually found in the range of 3000-3100 cm^{-1} [50]. In individual MA, the asymmetric/symmetric stretching vibrations spectra were calculated at 3007/2956 cm^{-1} corresponding to IR/Raman spectra at 2990/2951 cm^{-1} in Raman spectrum region. The same asymmetric/symmetric $C29H_2$ group stretching vibrations of monomer/ (monomer+1MA) were calculated at 3013/3014 cm^{-1} with Raman peak at 3016 cm^{-1}. The $C29H_2$ group symmetric vibrations were calculated at 2960/2957 cm^{-1} corresponding to Raman peak at 2970 cm^{-1}.

4.4 Quantum theory of atoms in molecules (QTAIM)

Richard F. W. Bader proposed quantum theory of atoms in molecules (QTAIM) to focus on chemically relevant information and nature of structural bond based on electron density (ρ) and bond critical points (BCPs) [51]. QTAIM method used the topological features of the density of electrons to describe properties at atomic level as well as chemical bonds in molecules [52]. This

theory is also applied to explain the properties of hydrogen bon interactions and hydrogen-hydrogen bonds [53]. Dihydrogen bonds exist in molecules chrysene and phenanthrene. In these molecules, the distance between two ortho hydrogens is shorter than their van der Waals radii and a bond path is identified between them [54]. The AIM analysis reveals the nature and strength of covalent and non-covalent interactions of molecules. Koch and Popelier et al. define existence and nature of hydrogen bonds as; BCP for donor (D)···acceptor (A), ($\nabla^2\rho_{BCP}$) lies in the range of 0.024-0.139 a.u. and the ρ_{BCP} within the range 0.002-0.040 a.u. [55]. The insights of characterization of hydrogen bond interactions were revealed by Rozas et al. as follows: (i) ($\nabla^2\rho_{BCP}$) < 0 and H_{BCP} < 0; for covalent nature and strong bond (ii) ($\nabla^2\rho_{BCP}$) > 0 and H_{BCP} < 0; For partially covalent and medium nature (iii) ($\nabla^2\rho_{BCP}$) > 0 and H_{BCP} > 0; for electrostatic and weak nature, (iv) It was pointed out that the bond distance of two interacting atoms should be smaller than the sum of van der Waals radii of these atoms [56]. Desiraju provides a method to interpret the weak (non-conventional) strong (conventional) hydrogen bonding, also C-H…O hydrogen bonds consists biological importance and are responsible for supramolecular synthesis and packing of crystal structure [57]. Topological and geometrical parameters like electron density (ρ_{BCP}) and Laplacian of the electron density (∇^2_{BCP}) at the bond critical points are used for characterization of the strength of hydrogen bonds in molecules.

The molecular graphs showing interactions in monomer and (monomer+1MA) of cocrystal are given in Figs. S10 and 7, respectively. The calculated topological and geometrical parameters for inter- and intramolecular hydrogen bond interactions of monomer and (monomer+1MA) of CAF-MA cocrystal are listed in Tables S7 and 2, respectively. The geometrical criteria for the existence of hydrogen bonds in monomer and (monomer+1MA) model of cocrystal, are tabulated in Tables S8 and S9, respectively.

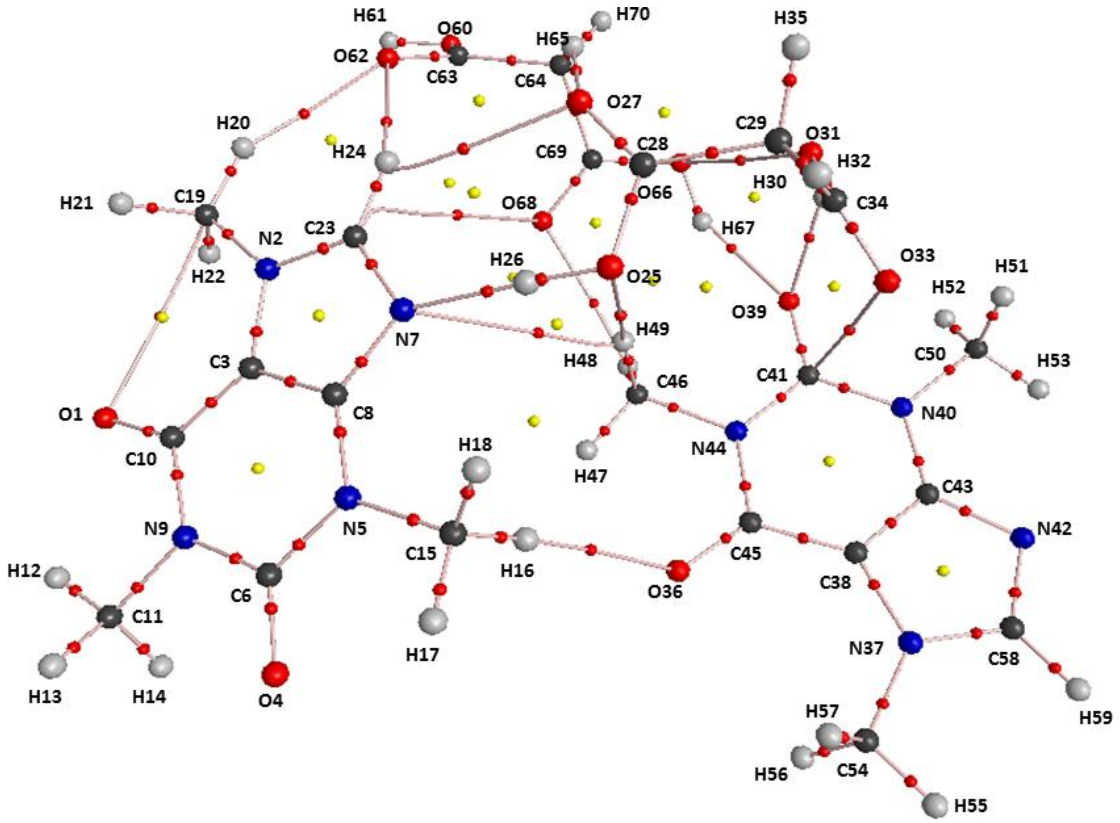

Fig. 7. Molecular graph of (monomer+1MA) of cocrystal: ring critical points (small yellow sphere), bond critical points (small red spheres) and bond paths (pink lines).

Table 2 Geometrical parameter (bond-length) and topological parameters for bonds of interacting atoms of intermolecular hydrogen bonding of (monomer+1MA) of CAF-MA cocrystal: electron density (ρ_{BCP}), Laplacian of electron density ($\nabla^2\rho_{BCP}$), electron kinetic energy density (G_{BCP}), electron potential energy density (V_{BCP}), total electron energy density (H_{BCP}) at bond critical point (BCP) and estimated interaction energy (E_{int}).

Hydrogen bonds	Bond-length (Å)	ρ_{BCP} (a.u.)	$\nabla^2\rho_{BCP}$ (a.u.)	G_{BCP} (a.u.)	V_{BCP} (a.u.)	H_{BCP} (a.u.)	E_{int} (kcal mol^{-1})
(O25-H26···N7)	1.6455	0.0598	0.1048	0.0157	-0.0576	-0.0419	-18.0723
(O66-H67···O39)	1.8592	0.0277	0.1104	-0.0021	-0.0233	-0.0254	-7.3105
(O31-H32···O39)	1.9385	0.0246	0.0899	-0.0017	-0.0197	-0.0214	-6.1810
(C19-H20···O62)	2.3663	0.0102	0.0361	-0.0014	-0.0062	-0.0076	-1.9453
(C23-H24···O62)	2.4497	0.0093	0.0312	-0.0011	-0.0055	-0.0066	-1.7256
(C46-H49···O68)	2.6055	0.0085	0.0292	-0.0010	-0.0052	-0.0062	-1.6315

(C64-H65⋯O27)	2.4502	0.0085	0.0291	-0.0011	-0.0051	-0.0062	-1.6001
(C15-H16⋯O36)	2.5410	0.0007	0.0233	-0.0008	-0.0042	-0.0050	-1.3178
(C23-H24⋯O27)	2.6560	0.0070	0.0241	0.0051	-0.0042	-0.0009	-1.3178
(C46-H48⋯O25)	2.9208	0.0038	0.0123	-0.0005	-0.0022	-0.0027	-0.6903
(C46-H48⋯N7)	3.2435	0.0027	0.0088	-0.0004	-0.0013	-0.0017	-0.4079

From Table S7 and S8, it is clear that in monomer model of cocrystal, the intermolecular hydrogen bond interactions; (O25-H26⋯N7) (1.7011 Å), (O31-H32⋯N42) (1.7243 Å), (C58-H59⋯O33) (2.3418 Å) and (C23-H24…O27) (2.3543 Å) possess medium and partially covalent nature, since ($\nabla^2\rho_{BCP}$) > 0 and H_{BCP} < 0. The intermolecular hydrogen bond (O25-H26⋯N7) with maximum intermolecular interaction energy for -14.9347 kcal mol^{-1}, is the strongest conventional hydrogen bond in monomer model.

Similarily, in (monomer+1MA) of CAF-MA cocrystal (as shown in Fig. 7), the order of hydrogen bonds were as follows; (O25-H26⋯N7) > (O66-H67⋯O39) > (O31-H32⋯O39) > (C19-H20⋯O62) > (C23-H24⋯O62) > (C46-H49⋯O68) > (C64-H65⋯O27) > (C15-H16⋯O36) > (C23-H24…O27) >(C46-H48⋯O25) > (C46-H48⋯N7), were medium and partially covalent nature, as ($\nabla^2\rho_{BCP}$) > 0 and H_{BCP} < 0 (as given in Table 2 and S9). In this model, (O25-N26⋯N7), (O66-H67⋯O39) and (O31-H32⋯O39) were conventional hydrogen bonds with interaction energies -18.0723, -7.3105 and -6.1810 kcal mol^{-1}, respectively. The non-coventional hydrogen bonds; (C19-H20⋯O62), (C23-H24⋯O62), (C46-H49⋯O68), (C64-H65⋯O27), (C15-H16⋯O36), (C23-H24⋯O27), (C46-H48⋯O25) and (C46-H48⋯N7) were found to be in the ranges -1.9453 to -0.4079 kcal mol^{-1}, showing the strength of hydrogen bonds, as per Desiraju criteria [74].

4.5 Natural bond orbital (NBO) analysis

NBO analysis is a method which provides a chemical intuitive understanding of bonds and electronic structure of molecules [58]. NBO analysis is fruitful approach to reveal the hybridization, covalence effects, charges, van der Waal and donor-acceptor interactions within and between molecules to interpret structure and chemical reactivity [59]. The NBO method provides donor-acceptor stabilization energies as well as chemical behavior and properties of molecules. The higher the value of second order stabilization energy; the electron donor-acceptor interaction will be stronger, also represents the larger range of structure and conjugation of molecules [60].

The second-order micro-disturbance theory of the Fock Matrix, the selected inter- and intramolecular interactions between filled electron donor and empty acceptor with $E^{(2)}$ of monomer and (monomer+1MA) were given in Tables S10 and S11,respectively. It could be clear from the Table S10, that the hyperconjugative charge transfers within σ(C19-H22) bonding to antibonding orbital π*(N2-C19) with $E^{(2)}$ value 236.95 kcal mol^{-1} denotes significant stabilization within CAF molecule in monomer model. Such types of interactions were present in various molecules [61, 62].

Another charge transfer interactions from unit 1 (CAF) to unit 2 (MA); n(1)N7 → σ*(O25-H26), showed a stabilization energy of 35.06 kcal mol^{-1}. The other charge transfer from unit 2 (MA) to unit 1 (CAF) in between lone pair n(1)O27 to anti bonding orbital σ*(C23-H24) highlighting the strength of n → σ* interactions, which influence its reactivity and stability. The charge transfer within unit 2 (MA), n(2)O25 → π*(O27=C28) and n(2)O31 → π *(O33=C34) both having $E^{(2)}$ values 68.68 kcal mol^{-1}, responsible for stabilization and formation of MA. Charge transfer interactions from unit 2 (MA) to unit 3 (CAF); n(1)O33 → σ*(C58-H59) with stabilization energy 1.08 kcal mol^{-1}. This intermolecular interaction reveals the presence of

classical (weak) hydrogen bonding (C58-H59⋯O33) in between CAF and MA. The other interaction between unit 3 (CAF) to unit 2 (MA) i.e. n(1)N42 → σ*(O31-H32) with $E^{(2)}$ value 35.06 kcal mol^{-1}, leading to the presence of strong hydrogen bond (N42⋯H32-O31) between CAF and MA (Fig. 2). The strongest charge transfer interaction within unit 3 (CAF); n(2)N42 → π*(N37-C58) with highest stabilization energy 154.87 kcal mol^{-1}, which provides extra stability to the CAF-MA cocrystal.

In similar way, the intermolecular charge transfer interactions between (monomer+1MA) of cocrystal; from unit 1 (CAF) to unit 2 (MA), from unit 1 (CAF) to unit 3 (CAF), from unit 1 (CAF) to unit 4 (MA), from unit 2 (MA) to unit 1 (CAF), from unit 2 (MA) to unit 3 (CAF), from unit 2 (MA) to unit 4 (MA), from unit 3 (CAF) to unit 1 (CAF), from unit 3 (CAF) to unit 2 (MA), from unit 3 (CAF) to unit 4 (CAF), from unit 4 (CAF) to unit 1 (CAF), From unit 4 (CAF) to unit 2 (MA) and from unit 4 (MA) to unit 3 (CAF); such as n(1)N7 → σ*(O25-H26), σ(C15-H16) → π*(O36=C45), σ(C15-H16) → π*(O36=C45), σ(C15-H18) → π*(O68=C69), n(1)O27 → σ*(C23-H24), n(2)O33 → π*(O39=C41), n(1)O27→ σ*(C64-H65), n(1)O36 → σ*(C15-H16), π(O39=C41) → σ*(O31-H32), n(1)O39 → σ*(O66-H67), n(1)O62 → σ*(C19-H20), n(2)O66 → σ*(O31-H32), n(2)O68 → σ*(C46-H49), with $E^{(2)}$ values of 48.15, 0.06, 0.11, 0.42, 0.47, 0.80,0.53, 3.88, 7.23, 1.15, 0.10, 0.28 kcal mol^{-1}, respectively. Additionally the intramolecular hydrogen bonding σ(O4=C6) → π*(N5-C6), n(2)O25 → π*(O27=C28), n(1)N37 → π*(N42-C58) and n(2)O60 → π*(O62=C63), respectively, with the $E^{(2)}$ values 167.33, 71.79, 81.76 and 58.66 kcal mol^{-1}, respectively, provide potential of extra stabilization of cocrystal (given in Table S11).

4.6 HOMO-LUMO analysis

HOMO-LUMO analysis provides the molecular properties, charge densities and distribution of molecules [63]. HOMO represents electron donating and LUMO as electron accepting tendency. These parameters also provide chemical reactivity of molecules [64], whereas the HOMO-LUMO energy gap (ΔE) provides insights into the chemical stability of molecules and charge transfer interactions. The higher ΔE shows a system has high chemical reactivity (low stability) and vice versa [65]. The detailed descriptions are provided in Supplementary information file.

4.7 Chemical reactivity descriptors

DFT methods are often used for elucidation of molecular structures and physicochemical properties [66]. The parameters such as ionization (I), electron affinity (A), electronegativity (χ), chemical potential (μ), global hardness (η), global softness (S) and electrophilicity index (ω) effectively predict chemical stability and reactivity of molecules [67]. The chemical reactivity descriptors (global and local) with the calculated parameters were described in Supplementary information file and given in Table S12.

4.8 Molecular electrostatic potential surface (MESP)

The MESP V(r) data can be derived from a quantum chemical DFT method that probably used to interpret and predict the various intermolecular hydrogen bonding, active (electrophilic and nucleophilic) binding sites and chemical reactivity of molecular systems [68, 69]. MESP maps are described by consisting of colors ranging from red to blue showing negative and positive sites, respectively. Yellow color represents less negative potential than that of red. Green color is the region representing neutral potentials. The red region in the MESP map is indicates an extremely negative (red) region that undergoes nucleophilic reactions. Similarly, the positive (blue) region is likely prone to attribute electrophilic reactions. Figs. S15, S16, S17 and 8

represent the resultant MESP maps of CAF, MA, monomer and (monomer+1MA) of CAF-MA cocrystal, respectively.

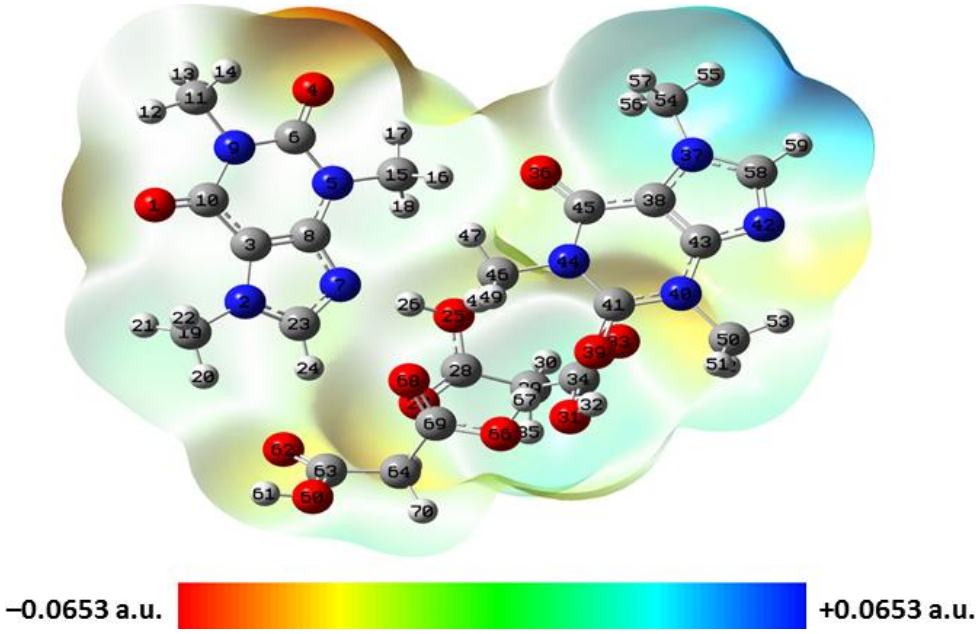

Fig. 8. Molecular electrostatic potential (MESP) formed by mapping of total density over electrostatic potential in the gas phase for (monomer+1MA) of CAF-MA cocrystal.

In MESP of CAF, the electron cloud concentrated at the two carbonyl groups; (C4=O10), (C8=O9) and N atom of imidazole ring of CAF appear as red region i.e. attributed to the electron delocalization and electron resonance feature present in the individual CAF. Secondly, the built up structure of CAF are localized by a light blue color in the methyl ($C13H_3$) and (C14-H15) of imidazole ring, representing slightly positive regions. This suggests that the hydrogen atom is distributed that nearly present in CAF, except for the sites containing N and O atoms. O atom adds a red color into the map instead of yellow as in N, as O is more electronegative than N (shown in Fig. S15). In MESP of MA (Fig. S16), hydroxyl groups (O2-H3), (O5-H6) and ($C8H_2$) are surrounded by blue region, indicating that is most likely to undergo electrophilic reactions.

Whereas localized in red color appeared at carbonyl groups; (C7=O1) and (C11=O4), indicates a positive potential around it hence susceptible for nucleophilic reactions.

Similarly, in the monomer of CAF-MA cocrystal (Fig. S17), carbonyl groups; (C6=O4), (C10=O1), (C41=O39) and (C45=O36) of CAF were present in red region, hence suitable for electrophilic attack, whereas blue region of methyl groups ($C19H_3$), ($C15H_3$), ($C11H_3$), ($C46H_3$), ($C50H_3$) and ($C54H_3$) of CAF were suitable for nucleophilic attacks, due to location into the blue region. Additionally, the nucleophilicity/electrophilicity of N7/H24, N42/H59 atoms of CAF and electrophilicity/nucleophilicity of H26/O27, H32/O33 atoms of MA were neutralized (green region) due to the presence of intermolecular hydrogen bonding; (N7···H26-O25), (C23-H24···O27), (N42···H32-O31) and (C58-H59···O33), respectively in between CAF and MA. Hence, it is a good indicator of structure-reactivity of two constituents CAF (API) and MA (coformer).

Similarily, from Fig. 8, in the (monomer+1MA) of CAF-MA cocrystal, the electrophilicity of ($C46H_3$) of pyrimidine ring and nucleophilicity of (C41=O39) of CAF were neutralized due to intermolecular hydrogen bondings; (C46-H49···O68) and (O66-H67···O39).

4.9 Drug likeness and molar refractivity

Lipinski's rule of five (RO5) is most likely used for the characterization of the drug-like compounds [70,71]. For those likely to be having conditions of absorption or permeability issues; at least two rules must be followed: (i) Molecular weight (MW) ≤ 500 Da, (ii) water partition coefficient (log P) ≤ 5, (iii) Number of hydrogen bond donors (NHD) ≤ 5, (iv) Number of hydrogen bond acceptors (NHA) ≥ 10 [70]. The drugs which follow these rules attain a higher

probability of being absorbed through gastrointestinal tract and reaching the intended targets [72].

According to the rules of set given by Veber, the molecules having; (i) molar refractivity (MR) values within 40 to 130 e.s.u., (ii) the molecular weight of 180-500 g mol^{-1}, (iii) the number of atoms lie between 20-70. These are the essential properties of drug candidates related to absorption and permeability [73].

The calculated MR values of CAF, monomer and (monomer+1MA) of cocrystal 30.35, 78.10 and 87.79 e.s.u., respectively. The molecular weights of CAF and CAF-MA cocrystal are 194.2 and 492.46 g mol^{-1}, respectively. Additionally, the numbers of atoms in CAF and monomer model of cocrystal are 24 and 59, respectively. Hence, as per above criteria, it is noteworthy that CAF and CAF-MA cocrystal interplay good correlation of these rules and hence, potential discriminant for drug design and evaluation (stating these as drug-like molecules).

5. Conclusions

A caffeine-malonic acid (CAF-MA) cocrystal was successfully prepared by solvent-assisted grinding and comprehensively characterized using PXRD, FT-IR, FT-Raman. A detailed DFT calculations were performed at the CAM-B3LYP/6-311++G(d,p) level of theory. A better agreement between the experimental and simulated PXRD patterns confirmed the formation and structural reliability of the cocrystal. Spectroscopic and computational analyses consistently demonstrated that the cocrystal formation is governed by a well-defined network of intermolecular hydrogen bonds, which significantly influences its structural and electronic properties. Vibrational study showed that mainly CN group of CAF and OH and C=O groups of

MA were involved in the formation of intermolecular hydrogen bonding between caffeine and malonic acid. AIM and NBO analyses revealed the nature and relative strength of these interactions, identifying the (O-H···N) and (O-H···O) hydrogen bonds as the dominant stabilizing interaction responsible for the enhanced stability of the cocrystal assembly. Furthermore, frontier molecular orbital and MESP analyses showed that cocrystallization modifies the electronic distribution and molecular reactivity of caffeine through intermolecular interactions. The HOMO-LUMO energy gap of the CAF–MA molecular complex (monomer +1MA) is smaller than that of the isolated CAF molecule, indicating a comparatively higher electronic reactivity of the molecular complex. Overall, this combined experimental and theoretical study provides a comprehensive understanding of the intermolecular interactions governing CAF-MA cocrystal formation and offers valuable insights for the rational design and optimization of pharmaceutical cocrystals with tailored physicochemical properties.

Acknowledgments

AS acknowledges the Department of Science and Technology, New Delhi, India for the Women Scientist Scheme (WOS A) for Research in Basic/Applied Sciences, award no. DST/WOS-A/CS-110/2021. PV and AS are thankful to the Central Facility for Computational Research (CFCR), University of Lucknow, Lucknow, India. PV is thankful to PAIR Network of SAKSHAM funded by Anusandhan National Research Foundation), India, through grant ANRFPAIR/2025/000018/PAIR, administered and mentored by IIT Indore. The authors gratefully acknowledge Dr. Manishkumar R. Shimpi (https://orcid.org/0000-0001-7469-4197) for preparing and providing the cocrystal material used in this study.

Author contribution

P.V. prepared all figures, carried out writing- original draft preparation, methodology and software. A.S. insured quality check and correction. P.P. contributed to manuscript editing and

writing. P.T. contributed to conceptualization, supervision and validation. U.S. contributed to data interpretation.

Funding This research did not receive funding.

Data availability statement All data generated or analysed during this study are included in this published article [and its supplementary information files].

Declarations

Ethics approval and consent to participate

Not applicable.

Consent for publication

Not applicable.

Competing interests

The authors declare no competing interests.

References

[1] Edwards PT, Saunders LK, Pallipurath AR, Britton AJ, Willneff EA, Shotton EJ, Schroeder SL. Proton transfer on the edge of the salt/cocrystal continuum X-ray photoelectron spectroscopy of three isonicotinamide salts. Cryst Growth Des. 2021;21:6332-6340.

[2] Ouyang J, Xing X, Zhou L, Zhang C, Heng JY. Cocrystal design of vanillin with amide drugs Crystal structure determination, solubility enhancement, DFT calculation. Chem Eng Res Des. 2022;183:170-180.

[3] Ouyang J, Liu L, Li Y, Chen M, Zhou L, Liu Z, Shehzad H. Cocrystals of carbamazepine Structure, mechanical properties, fluorescence properties, solubility, dissolution rate. Particuol. 2024;90:20-30.

[4] Roy P, Pey N, Kumari N, Baidya R, Mary YS, Ghosh A. Development of sulfamethoxazole-succinimide cocrystal by mechanochemical cocrystallization–An insight into spectroscopic,

electronic, chemical conformation physicochemical properties. Chem Eng Res Des. 2022;185:446-457.

[5] Sakhiya DC, Borkhataria CH. A review on advancement of cocrystallization approach and a brief on screening, formulation and characterization of the same. Heliyon. 2024;10:e29057.

[6] Pantwalawalkar J, Kale N, Nangare S, Patil S, Pawar S, Jadhav N. Pharmaceutical cocrystals: unlocking the potential of challenging drug candidates. J Drug Deliv Sci Technol. 2025;104: 106572.

[7] Sun Z, Lin B, Yang X, Zhao B, Zhang H, Dong Q, Zang H. Review of the application of Raman spectroscopy in qualitative and quantitative analysis of drug polymorphism. Curr Top Med Chem. 2023;23:1340-1351.

[8] Eshbekova N, Sowndarya A, Thangadurai TD, Lee YI. Recent advancements in Raman instrumentation and capabilities for pharmaceutical and biomedical applications. Appl Spectrosc Rev. 2024;59:798-849.

[9] Huang S, Deng H, Wei X, Zhang J. Progress in application of terahertz time-domain spectroscopy for pharmaceutical analyses. Front Bioeng Biotechnol. 2023;11:1219042.

[10] Du Y, Xue J, Hong Z. Raman and terahertz spectroscopic characterization of solid-state cocrystal formation within specific active pharmaceutical ingredients. Curr Pharm Des. 2020;26: 4829-4846.

[11] Alsirawan MB, Lai X, Prohens R, Vangala VR, Pagire SK, Shelley P, Paradkar A. Solid-State Competitive Destabilization of Caffeine Malonic Acid Cocrystal Mechanistic Kinetic Investigations. Cryst Growth Des. 2020;20: 7598-7605.

[12] Guan H, Sun H, Zhao X. Application of density functional theory to molecular engineering of pharmaceutical formulations. Int J Mol Sci. 2025;26:3262.

[13] Singh I, El-Emam AA, Pathak SK, Srivastava R, Shukla VK, Prasad O, Sinha L. Experimental theoretical DFT (B3LYP, X3LYP, CAM-B3LYP M06-2X) study on electronic structure, spectral features, hydrogen bonding solvent effects of 4-methylthiadiazole-5-carboxylic acid. Mol Simul. 2019;45:1029-1043.

[14] Li M, Reimers JR, Ford MJ, Kobayashi R, Amos RD. Accurate prediction of the properties of materials using the CAM-B3LYP density functional. J Comput Chem. 2021;42:1486-1497.

[15] Mucha W, Bąkowicz J, Malik M, Morzyk-Ociepa B. Structural, Vibrational Spectroscopic Theoretical (DFT) Studies of 4-Chloro- 5-Chloro-7-azaindole-3-carbaldehydes. Cryst. 2024;14: 631.
[16] Nartowski KP, Khimyak YZ, Berry DJ. Tuning the spontaneous formation kinetics of caffeine: malonic acid co-crystals. CrystEngComm. 2016;18:2617-2620.
[17] Otsuka Y, Ito A, Takeuchi M, Tanaka H. Dry mechanochemical synthesis of caffeine/oxalic acid cocrystals and their evaluation by powder X-ray diffraction and chemometrics. J Pharm Sci. 2017;106:3458-3464.
[18] Trask AV, Motherwell WS, Jones W. Pharmaceutical cocrystallization engineering a remedy for caffeine hydration. Cryst Growth Des. 2005;5:1013-1021.
[19] Hawkins BA, Du JJ, Lai F, Stanton SA, Williams PA, Groundwater PW, Hibbs DE. An experimental theoretical charge density study of theophylline malonic acid cocrystallization. RSC Adv. 2022;12:15670-15684.
[20] Srivastava D, Fatima Z, Kaur CD, Mishra A, Nashik SS, Rizvi DA, Prasad R. Glibenclamide–malonic acid cocrystal with an enhanced solubility bioavailability. Drug Dev Ind Pharm. 2022;48:417-424.
[21] Leger JM, Alberola S, Carpy A. Structure cristalline du complexe 1 1 sulfacétamide–caffeine. Acta Crystallogr Sect B Struct Crystallogr. Cryst Chem. 1977;33:1455-1459.
[22] Craven BM, Gartl GL. The 2 1 crystal complex of 5, 5-diethylbarbituric acid (barbital) caffeine. Acta Crystallogr Sect B Struct Crystallogr Cryst Chem. 1974;30:1191-1195.
[23] Mukaida M, Watanabe Y, Sugano K, Terada K. Identification physicochemical characterization of caffeine–citric acid co-crystal polymorphs. Eur J Pharm Sci. 2015;79:61-66.
[24] Verma P, Srivastava A, Srivastava K, Tandon P, Shimpi MR. Molecular structure, spectral investigations, hydrogen bonding interactions reactivity-property relationship of caffeine-citric acid cocrystal by experimental DFT approach. Front Chem. 2021;9:708538.
[25] Shimpi MR, Childs SL, Boström D, Velaga SP. New cocrystals of ezetimibe with L-proline imidazole. CrystEngComm. 2014;16:8984-8993.
[26] Öztürk N, Özdemir T, Alpaslan YB, Gokce H, Alpaslan G. Experimental (FT-IR, Raman NMR) theoretical (B3LYP, B3PW91, M06-2X CAM-B3LYP) analyses of PTert-butylphenyl salicylate. Bilgesci. 2018;2:56-73.

[27] Olsen ST, Elm J, Storm FE, Gejl AN, Hansen AS, Hansen MH, Mikkelsen KV. Computational methodology study of the optical thermochemical properties of a molecular photoswitch. J Phys Chem A. 2015;119:896-904.
[28] Frisch MJ, et al., Gaussian 09, Revision, Gaussian, Inc., Wallingford CT, 2009.
[29] Frisch A, Nielson AB, Holder AJ. Gaussview user manual. Gaussian Inc., Pittsburgh, PA, 2000.
[30] Petitjean H, Giard A, Flament JP, Berthomieu C, Berthomieu D. Fast vibrational analysis of molecular systems. J Comput Chem. 2024;45:2374-2382.
[31] Pulay P, Fogarasi G, Pang F, Boggs JE. Systematic ab initio gradient calculation of molecular geometries, force constants, dipole moment derivatives. J Am Chem Soc. 1979;101:2550-2560..
[32] Martin JML, Van Alsenoy C. Gar2ped, University of Antwerp, Belgium, 1995.
[33] Keith TA. AIMALL Version 090201 TK Gristmill Software Overland Park, KS, 2009.
[34] Bader RFW, J. R. Cheeseman, 2000. In AIMPAC, 2000.
[35] Espinosa E, Molins E, Lecomte C. Hydrogen bond strengths revealed by topological analyses of experimentally observed electron densities. Chem Phys Lett. 1998;285:170-173.
[36] Mary YS, Raju K, Panicker CY, Al-Saadi AA, Thiemann T, Van Alsenoy C. Molecular conformational analysis, vibrational spectra, NBO analysis first hyperpolarizability of (2E)-3-phenylprop-2-enoic anhydride based on density functional theory calculations. Spectrochim Acta A Mol Biomol Spectrosc. 2014;128:638-646.
[37] Pal R, Chattaraj PK. Electrophilicity index revisited. J Comput Chem. 2023;44:278-297.
[38] Shankar R, Senthilkumar K, Kolaivel P. Calculation of ionization potential chemical hardness A comparative study of different methods. Int J Quantum Chem. 2009;109:764-771.
[39] Saleh ZA, Taha DK. Calculation of Ionization energies, electron affinities, hardnesses electro negativites, using many bases set of many methods. Int J Sci Eng. 2014;5:727-4729.
[40] Al Nabulsi AR, Heidar-Zadeh F, Ayers PW. Systematic Testing of the Maximum Hardness Minimum Electrophilicity Principles. J Phys Chem A. 2026;130:3221-3232.

[41] Baiz AR, Błasiak B, Bredenbeck J, Cho M, Choi JH, Corcelli SA, Zanni MT. Vibrational spectroscopic map, vibrational spectroscopy, and intermolecular interaction. Chem Rev. 2020;120:7152-7218.

[42] Rahmani R, Perveen F, Benhalima N, Djafri A, Khelloul N, Chouaih A, Goumri Said S. FTIR, NMR and UV–visible spectral investigations, theoretical calculations, topological analysis, chemical stablity, and molecular Docking study on novel bioactive compound: the 5-(5-Nitro Furan-2-Ylmethylen), 3-N-(2-Methoxy Phenyl), 2-N′-(2-Methoxyphenyl) Imino thiazolidin-4-One. Polycycl Aromat Comp. 2023;43:4685-4706.

[43] Lehmann CW, Stowasser F. The crystal structure of anhydrous β-caffeine as determined from X-ray powder-diffraction data. Eur J Pharm Sci. 2007;13:2908-2911.

[44] Gopalan RS, Kumaradhas P, Kulkarni GU, Rao CNR. An experimental charge density study of aliphatic dicarboxylic acids. J Mol Struct. 2000;521:97-106.

[45] Rodrigues-Oliveira AF, Ribeiro FWM, Cervi G, Correra TC. Evaluation of common theoretical methods for predicting infrared multiphotonic dissociation vibrational spectra of intramolecular hydrogen-bonded ions. ACS omega. 2018;3:9075-9085.

[46] Ramkumaar GR, Srinivasan S, Bhoopathy TJ, Gunasekaran S, Charles J, Ramesh J. Molecular structure, vibrational spectra, UV–vis, NBO, NMR analyses on nevirapine using ab initio DFT methods. J Theor Appl Phys. 2013;7:51.

[47] Avcı D, Cömert HE, Sönmez F, Dege N, Tamer Ö, Atalay Y. Comparative assessment of structure–property relationships of new Cu (II) complex in selected density functionals. Spectrochim Acta A Mol Biomol Spectrosc. 2024;305:123489.

[48] Socrates G. Infrared Raman characteristic group frequencies tables charts, John Wiley Sons, Inc., New York, 2004.

[49] Ridha SM, Saleh ZA, Askar FW. Theoretical Experimental Study for FT-IR UV/VIS Spectra of 1, 4-diphenyl-3-(phenylammonio)-1H-1, 2, 4-triazolium (inner salt) by Using DFT Approach. Phys Chem. 2015;5:6-15.

[50] Stuart BH. Infrared spectroscopy fundamentals applications, John Wiley & Sons, Inc., New York, 2004.

[51] Bader RF. A quantum theory of molecular structure its applications. Found Chem. 1991;91:893-928.

[52] Alsaab HO. DFT QTAIM analysis of fluorenol fluorenone in molecular nanoelectronics. Sci Rep. 2025;15:21452.
[53] Grabowski SJ, Małecka M. Intramolecular H-bonds DFT QTAIM studies on 3-(aminomethylene) pyran-2, 4-dione its derivatives. J Phys Chem A. 2006;110:11847-11854.
[54] Grabowski SJ. Triel Bonds─ Interactions without Borders, Similarly as Hydrogen Bonds. Cryst Growth Des. 2025;25:4539-4552.
[55] Koch U, Popelier PL. Characterization of CHO hydrogen bonds on the basis of the charge density. J Phys Chem. 1995;99:9747-9754.
[56] Rozas I, Alkorta I, Elguero J. Behavior of ylides containing N, O, C atoms as hydrogen bond acceptors. J Am Chem Soc. 2000;122:11154-11161.
[57] Desiraju GR. Hydrogen bonds other intermolecular interactions in organometallic crystals. J Chem Soc Dalton Trans. 2000;21:3745-3751.
[58] Agwupuye JA, Louis H, Unimuke TO, David P, Ubana EI, Moshood YL. Electronic structure investigation of the stability, reactivity, NBO analysis, thermodynamics, the nature of the interactions in methyl-substituted imidazolium-based ionic liquids. J Mol Liq. 2021;337:116458.
[59] Reed AE, Curtiss LA, Weinhold F. Intermolecular interactions from a natural bond orbital, donor-acceptor viewpoint. Chem Rev. 1988;88:899-926.
[60] Hassan U, Sumrra SH. Structure-based screening of sp 2 hybridized small donor bridges as donor acceptor switches for optical photovoltaic applications DFT way. J Mol Model. 2024;30:36.
[61] Saral A, Manikan S, Javed S, Muthu. Vibrational spectra, molecular level solvent interaction, stabilization, donor-acceptor energies, thermodynamic, non-covalent interaction electronic behaviors of 6-Methoxyisoquinoline-anti tubercular agent. Chem. Phys Impact. 2024;8:100392.
[62] Paneru TR, Chaudhary MK, Tandon P, Chaudhary T, Joshi BD. Theoretical study on molecular stability, reactivity, drug potential of cirsilineol from DFT molecular docking methods. Chem Phys Impact. 2024;8:100641.
[63] Gil DM, Lestard MD, Estévez-Hernández O, Duque J, Reguera E, Quantum chemical studies on molecular structure, spectroscopic (IR, Raman, UV–Vis), NBO Homo–Lumo

analysis of 1-benzyl-3-(2-furoyl) thiourea. Spectrochim Acta A Mol Biomol Spectrosc. 2015;145:553-562.

[64] Huang Y, Rong C, Zhang R, Liu S. Evaluating frontier orbital energy HOMO/LUMO gap with descriptors from density functional reactivity theory. J Mol Model. 2017;23:3.

[65] Miar M, Shiroudi A, Pourshamsian K, Oliaey AR, Hatamjafari F. Theoretical investigations on the HOMO–LUMO gap global reactivity descriptor studies, natural bond orbital, nucleus-independent chemical shifts analyses of 3-phenylbenzo [d] thiazole-2 (3 H)-imine its para-substituted derivatives Solvent substituent effects. J Chem Res. 2021;45:147-158.

[66] Nieto-Draghi G, Fayet B, Creton X, Rozanska P, Rotureau JC, de Hemptinne, Adamo C. A general guidebook for the theoretical prediction of physicochemical properties of chemicals for regulatory purposes. Chem Rev. 2015;115:13093-13164.

[67] Vijayalakshmi R, Anantharaj R, Brinda Lakshmi A. Evaluation of Chemical Reactivity Stability of Ionic Liquids Using Ab Initio COSMO-RS model. J Comput Chem. 2020;41:885-912.

[68] Gadre SR, Suresh CH, Mohan N. Electrostatic potential topology for probing molecular structure, bonding reactivity. Molecules. 2021;26:3289.

[69] Matta CF. Modeling biophysical biological properties from the characteristics of the molecular electron density, electron localization delocalization matrices, the electrostatic potential. J Comput Chem. 2014;35:1165-1198.

[70] Lipinski CA, Lombardo F, Dominy BW, Feeney PJ. Experimental and computational approaches to estimate solubility and permeability in drug discovery and development settings. Adv Drug Deliv Rev. 2012;64:4-17.

[71] Petit J, Meurice N, Kaiser C, Maggiora G. Softening the rule of five—where to draw the line?. Bioorg Med Chem. 2012;20:5343-5351.

[72] Doak BC, Over B, Giordanetto F, Kihlberg J. Oral druggable space beyond the rule of 5: insights from drugs and clinical candidates. Chem Biol. 2014;21:1115-1142.

[73] Veber DF, Johnson SR, Cheng HY, Smith BR, Ward KW, Kopple KD. Molecular properties that influence the oral bioavailability of drug candidates. J Med Chem, 2002;45:2615-2623.

Supplementary Files

This is a list of supplementary files associated with this preprint. Click to download.

- Table1.docx
- Table2.docx
- SupplementaryMaterial.docx